High efficiency removal of As(III) from waters using a new and friendly adsorbent based on sugarcane bagasse and corncob husk Fe-coated biochars

José Ignácio Z. Montero[a], Adnívia S.C. Monteiro[a,b], Erik S.J. Gontijo[a,c], Carolina C. Bueno[a], Minéia A. de Moraes[a], André H. Rosa[a,*]

[a] Sao Paulo State University (UNESP), Institute of Science and Technology, Av. Tres de Marco, 511, Alto da Boa Vista, CEP: 18087-180, Sorocaba, SP, Brazil
[b] Federal University of Sergipe (UFS), Postgraduate Program in Water Resources, Av. Marechal Rondon, s/n - Jd. Rosa Elze, 49100-000, Sao Cristovao, SE, Brazil
[c] UFZ-Helmholtz Centre for Environmental Research, Department Lake Research, Brueckstr 3a, 39114 Magdeburg, Germany

A B S T R A C T

Water contamination of As is a big issue in many areas around the globe. Therefore, cheap and efficient techniques are essential facing traditional treatment methods. Then, biochars (BC) emerged recently as material that can be used for As removal. However, research about efficiency of BC produced from local feedstock is still needed. The purpose of this study is to assess the efficiency of BC produced from sugarcane bagasse (SB) together with corncob husk (CH) with and without Fe(III) (BC$_{Fe}$) modification to be used for removal of As(III) from waters. The BC and BC$_{Fe}$ produced at different pyrolysis temperatures were characterised using FTIR and SEM/EDS. Adsorption capacities of BC and BC$_{Fe}$ were evaluated *via* batch adsorption, desorption and column tests and their performance was compared with adsorption using activated carbon. The results showed that Fe modification improve substantially the As(III) adsorption in a way that both BC$_{Fe-SB}$ and BC$_{Fe-CH}$ removed from 85% to 99.9% from 1000 µg/L As(III) solutions. Both materials fitted well in Langmuir model and the maximum adsorption capacity was 20 mg/g for BC$_{Fe-SB}$ and 50 mg/g for BC$_{Fe-CH}$. The adsorption kinetics of BC$_{Fe}$ was fast ($\leq$ 30 min) and it had a better performance than activated carbon. The column tests showed that the process is efficient even at high As(III) concentrations. The fast removal process and good removal results make the BC$_{Fe-SB}$ and BC$_{Fe-CH}$ attractive for *in situ* and commercial (filters) use, since time and efficiency are required in new technologies.

1. Introduction

Arsenic (As) contamination of aquatic systems is a worldwide problem that severely affects people and animals. The concern related to As comes from its prevalence and high toxicity, which depends on its chemical form (Jain and Ali, 2000). Generally, As(III) species are the most toxic followed by As(V) and organic species (Jain and Ali, 2000; Wang and Mulligan, 2006).

Weathering of rocks, leaching of soils and volcanic emissions are the main natural sources of As in aquatic systems (Smedley and Kinniburgh, 2002). Human activities like mining, smelting, fossil fuel combustion, waste disposal and use of some pesticides and herbicides also contribute to the input of this metalloid in the environment (Azizur Rahman and Hasegawa, 2012; Morin and Calas, 2006). The increasing amount of As released *via* anthropogenic sources boosts the world problems related to As chronic exposure, which can cause skin diseases and cancer (Sharma and Sohn, 2009). In this way, a cheap and efficient method to remove As from contaminated water and effluents is highly desirable.

Currently, the best known techniques for the removal of As and other contaminants from aquatic systems include processes such as (ad)sorption and ion-exchange using activated carbon/modified activated carbon and alumina, iron coated sand, ion-exchange resins (Asfaram et al., 2015; Bazrafshan et al., 2017; Cumbal et al., 2003; Dambies, 2005; Haron, 1997), biosorbents (chitin, chitosan, cellulose sponge (Guo and Chen, 2005; Muñoz et al., 2002), biomass (Ghimire et al., 2002; J. Kim et al., 2006; Pokhrel and Viraraghavan, 2006)) and nanoadsorbent (Asfaram et al., 2017a, 2018; Lata and Samadder, 2016; Qu et al., 2013), such as nanocrystalline magnetite (Mayo et al., 2007), graphene oxide (Chandra et al., 2010) and Mn$_{0.4}$Zn$_{0.6}$Fe$_2$O$_4$ nanoparticles (Asfaram et al., 2018). Some of other techniques used are coagulation, electrocoagulation (Nidheesh and Singh, 2017; Ratna Kumar et al., 2004; Thakur and Mondal, 2017), coprecipitation, phytoremediation (Leão et al., 2017; Natarajan et al., 2011), bioremediation (Gihring et al., 2001) and biofilters (Sharma and Sohn, 2009;

Vithanage et al., 2017), solvent extraction (Budinova et al., 2006), foam flotation (Kordmostafapour et al., 2006; Pacheco and Torem, 2002) and also membrane techniques, such as nanofiltration, reverse osmosis, and electrodialysis (Ballinas et al., 2004; Choong et al., 2007; D.H. Kim et al., 2006; Ungureanu et al., 2015).

Despite the good adsorption removal efficiency, materials used in most of these techniques are expensive and require a large amount of energy. Hence, easily available (available locally), cost-effective (processing required and treatment conditions) and efficient materials are required. The use of biochar (BC) as an adsorbent to remove As from water is classified as a low-cost adsorbent technique, making BC usage particularly advantageous when compared to the techniques described previously (Asfaram et al., 2017b). Other low-cost adsorbents can be obtained from industrial by-products/wastes chars and coals (Mohan and Chander, 2006), red mud (Genç et al., 2003; Soner Altundoğan et al., 2000), blast furnace slag (Ahn et al., 2003; Zhang and Itoh, 2005), fly ash (Diamadopoulos et al., 1993; Gupta et al., 2005), zeolites (Wang and Peng, 2010), clay minerals, coconut shells, wood char, lignin, petroleum coke, bone-char, peat, sawdust, carbon black, rice hulls, sugar, peach pits (Pollard et al., 1992) and sand (Ramakrishna et al., 2006). Besides the economic factor, agricultural products and by-products are preferable because the storage and handling of these types of wastes are easy and safe and they do not need specific operation and maintenance, and provide a noble destination for the organic load produced that could lead to accumulation of nutrients in the environment.

Surface area may not be a primary factor for adsorption on BC and, thus high surface area does not necessarily mean high adsorption capacity. Therefore, the adsorption of As probably depends on the surface chemistry (Corapcioglu and Huang, 1987). Hence, it is known that ligands as As oxyanions are adsorbed on iron hydroxide and aluminium sulphate flocs as Fe complexes (Hering, 1996). This given mechanism can be transferred to the adsorbent materials by chemical modification and thus improve the removal capacity of this type of contaminants. Consequently, the chemical modification of BC transforms it into an adsorbent with positive charge, which facilitates the As removal by the means of Coulombic interactions. Additionally, the presence of Fe groups in BC may impart a magnetic feature to the adsorbent that facilitates removal of contaminated water system (Dong et al., 2018).

This study aims to evaluate the capabilities of biochar and Fe-coated biochar produced from corncob husk (CH) and sugarcane bagasse (SB) of Brazilian crops to remove As(III) from highly contaminated aquatic systems. These feedstocks can be readily available, particularly in countries like Brazil and China, which have big sugarcane and/or maize crops (Bueno et al., 2017; Moraes et al., 2012). In addition, the use of leftover biomass from maize (corncob husk) and sugarcane (bagasse) production would minimise the waste generation and impact of these crops on the environment (Manochio et al., 2017). The As removal efficiency of Fe-coated biochars were also compared with commercially activated carbon. Furthermore, the efficiency of As removal by Fe-coated biochar in a column leaching experiment was tested.

2. Experimental

2.1. Biochar and Fe-coated biochar preparation

The corncob husk (CH) and sugarcane bagasse (SB) were washed with water and dried in a drying oven with mechanical air circulation at 80 ºC for 48 h. The material was crushed (Willey mill MA048) and the biomass powder (60 g) was pyrolyzed using a bed cylindrical reactor (0.82 cm^3) in a muffle furnace (EDGCON-3P). Four different biochars (BC) were produced after setting the pyrolysis temperature at 300, 400, 500 and 600 ºC with an increase rate of 10 ºC/min. The furnace was kept in the target temperature for 180 min (retention time) and it was cooled at room temperature for 12 h (overnight).

Fe-coated biochars (BC$_{Fe}$) were produced by immersing the biomass

in a FeCl$_3$ solution (2.5 mol/L) for 2 h. The mixture was then dried at 80 °C for 2 h in a drying oven with mechanical air circulation. The biomass modified with Fe was pyrolyzed in porcelain crucibles using the same treatments (4 different temperatures) and conditions used for unmodified BC.

All BC and BC$_{Fe}$ were passed through a 35-mesh sieve and stored in polypropylene bottles at room temperature until analysis.

2.2. Characterisation of biochar and Fe-coated biochar

To investigate the evolution of porosity and changes in elemental composition, the surfaces of the biochars and Fe-coated biochars were analysed by a scanning electron microscope (SEM) and by energy dispersive X-ray spectroscopy (EDS) (JEOL JSM-6010LA).

A Fourier transform infrared (FTIR) spectrometer (PerkinElmer® Spectrum 65 FTIR) with attenuated total reflection (ATR) was used to study the surface functional groups of all biochars. All spectra were obtained with 4 cm^{-1} resolution over spectral range from 4000 to 650 cm^{-1} (32 scans).

2.3. pH of zero point of charge (pH$_{zpc}$)

The pH of zero point of charge (pH$_{zpc}$) was determined from adding 0.5 mg of biochar in 50 mL of ultrapure water. The experiments were performed with BC and BC$_{Fe}$ from SB and CH (4 sets of experiments). The pH was adjusted in the range 2–12 (11 samples) using NaOH 0.10 mol/L and HCl 0.10 mol/L solutions for each biomass. All samples were shaken at 3 g at 25 ºC for 24 h. Measuring the pH of each sample and analysing the data (ΔpH × initial pH) it was found that the initial pH and the final pH were the same, which corresponds to the pH$_{zpc}$ (Mohan et al., 2014).

2.4. Adsorption kinetics and isotherms

Adsorption kinetics experiments of As(III) on BC and BC$_{Fe}$ produced at all pyrolysis temperatures (300, 400, 500 and 600 ºC) from SB and CH biomass were carried out by mixing 0.1 g of the adsorbent with 100 mL of 1000 μg/L As(III) solution in 125 mL erlenmeyers. The same procedure was carried out for commercially activated carbon for comparison. The erlenmeyers were shaken in a shaker for 24 h at 3 g at room temperature. Experiments were also performed without adsorbents to evaluate a possible precipitation of As. Visual MINTEQ software (freeware, version 3.0) was used to evaluate possible precipitation of As in the experiments under the same conditions. Aliquots (2 mL) were taken after 0, 1, 10, 20, 30, 45, 60, 90, 180, 300, 600 and 1440 min using syringes and immediately filtered through 0.45 μm pore size PVDF filters. All experiments were performed in duplicate at three different pH (4, 5 and 6). The As in the filtered samples were determined by inductively coupled plasma-atomic emission spectrometry (ICP OES, Agilent Technologies 700 Series).

The kinetic study provides important information regarding the reaction pathways and the mechanisms of sorption. The reaction rate and the adsorption mechanisms, for instance, play an essential role in water treatment process, since they determine the contact time necessary to the complete and efficient adsorption of the adsorbate on the adsorbent (Ho and McKay, 1999). Therefore, the pseudo-first order kinetic model and the pseudo-second order model were determined in order to investigate the sorption mechanisms of As(III) onto BC and BC$_{Fe}$. The equation used to describe the pseudo-first order kinetic model is (Eq. (1)) (Van Vinh et al., 2015):

$$log(q_e - q_t) = logq_e - (k_1/2.303)t, \tag{1}$$

where k$_1$ (mg/g.min) is pseudo-first order adsorption rate constant (from slopes of linear plot log(q$_e$ − q$_t$) × t), q$_e$ is the amount of adsorbate at the equilibrium time, q$_t$ is the amount of adsorbent at equilibrium time and t is the time.

The pseudo-second order model can be expressed by the equation (Eq. (2)) (Van Vinh et al., 2015):

$$t/q_t = 1/(k_2 q_e^2) + (1/q_e)t, \qquad (2)$$

where k_2 (mg/g.min) is the pseudo-second-order adsorption rate constant.

The amount of metals adsorbed (q, mg of metal/ g of adsorbent) on all BC_{Fe} (300 ºC) was assessed based on pH, contact time, concentration of adsorbent and adsorbate. The following equation (Eq. (3)) was used to calculate q (Mohan et al., 2007):

$$q = (C_0 - C_e)V/W, \qquad (3)$$

where C_0 and C_e are respectively the initial and equilibrium metal ion concentrations in solution (mg/L), V is the adsorbate volume and W is the adsorbent weight (g).

Adsorption isotherms of As(III) to BC were determined by mixing 0.1 g of BC_{Fe} at 300ºC in 100 mL of As(III) solutions of concentration ranging from 1 to 50 mg/L. The pH values of all treatments were adjusted to 4 and the samples were shaken in a shaker for 360 min at 3 g and 25 ºC. The experiment duration time was set to 360 min to assure that the adsorption equilibrium was established based on kinetic experiments results. Aliquots of the samples (2 mL) were taken and filtered through 0.45 µm pore size PVDF filters. All experiments were performed in duplicate.

The performance and isotherm parameters of BC_{Fe-CH} and BC_{Fe-SB} produced at 300 ºC were evaluated based on the nonlinear Langmuir and Freundlich models. The Langmuir isotherm model explains the adsorption processes in a homogeneous media, where all adsorption sites of the adsorbent have equal affinity to the adsorbate. This model is valid for a monolayer sorption mechanism and none of the binding sites of adsorbent affects its neighbours (Baig et al., 2014; Mohan et al., 2007). The equation (Eq. (4)) used to describe this nonlinear model is (Mohan et al., 2007):

$$q_e = Q^0 b C_e/(1 + b C_e), \qquad (4)$$

where q_e is the amount of solute adsorbed (µg/g); Q^0 is the monolayer adsorption capacity (µg/g); Ce is the equilibrium concentration of solute bulk solution (mg/L) and b is the constant linked to free energy.

In contrast to the Langmuir model, the nonlinear Freundlich model describes the adsorption processes in a heterogeneous media. Furthermore, this model is not valid for a monolayer sorption mechanism and it can only be applied from low to intermediate concentration levels (Mohan et al., 2007). The formula (Eq. (5)) used to describe this model is:

$$q_e = K_F C_e^{\frac{1}{n}}, \qquad (5)$$

where K_F is the relative adsorption capacity constant of the adsorbent (L/µg) and 1/n is the adsorption constant intensity.

2.5. Biochar mass influence on As(III) adsorption

The experiments performed with BC_{Fe} produced at 300 ºC both from CH and SB biomass to evaluate the influence of the mass of BC_{Fe} on removal of As(III). Five different amounts of BC_{Fe} (0.05, 0.1, 0.2, 0.4 and 0.5 g) were added to flasks with 100 mL solution of 1000 µg/L As (III). The pH values of all experiments were adjusted to 4 and the flasks were shaken in a shaker at 3 g at room temperature. Aliquots were taken at 0, 1, 10, 20, 30, 45, 60, 90, 180, 300 and 360 min and afterwards they were filtered through 0.45 µm membranes. As concentration was determined in an ICP-OES as described in Section 2.4.

2.6. Desorption and re-adsorption experiments

Batch desorption experiments were performed to verify if the adsorption of As(III) on biochars is reversible. This study consists of an adsorption followed by a desorption phase using the best conditions from previous tests (Sections 2.3–2.5). Briefly, 0.1 g of Fe-coated biochar (BC_{Fe-SB} and BC_{Fe-CH} produced at 300ºC) was added to 100 mL solution (pH 4) containing 1000 µg/L As(III). The mixture was shaken at 3 g for 300 min (adsorption phase). Extra adsorption experiments were performed to further investigate the interactions between As(III) and BC_{Fe} after adsorption. FTIR spectra of BC_{Fe} before and after As(III) adsorption were acquired (as Section 2.2) and afterwards compared.

After the sorption step, the supernatant was substituted by 100 mL solution containing 0.01 mol/L CaCl$_2$, as described by Huang et al. (1998) and Zhang et al. (2010). The suspensions were shaken at 3 g and aliquots were taken after 300 min (desorption phase). Afterwards, the samples were filtered through 0.45 µm membranes and the desorbed metalloid in the samples were measured using an ICP-OES. The desorption experiments with BC_{Fe-SB} and BC_{Fe-CH} were performed in triplicate.

After the desorption, a re-adsorption experiment of the BC_{Fe-SB} and BC_{Fe-CH} were performed using the same conditions of the first adsorption. The samples were filtered through 0.45 µm membranes and the desorbed metalloid in the samples were measured using an ICP-OES as described previously.

2.7. Influence of ionic strength on As adsorption

The influence of the ionic strength on As(III) adsorption was evaluated using the BC with the best removal rates and the best conditions as described in Section 2.6. Briefly, 0.1 g of BC (BC_{Fe-SB} and BC_{Fe-CH}) was added to 100 mL solution (pH 4) containing 1000 µg/L As(III). The experiments were performed in three different NaNO$_3$ concentrations: 0.01, 0.1 and 1 mol/L. The mixtures were shaken at 25 ˚C (3 g) and aliquots were taken at 0, 1, 10, 20, 30, 45, 60, 90, 180 and 300 min. The samples were filtered through 0.45 µm membranes and analysed in ICP-OES.

2.8. Column leaching experiment

A glass column (24 mm diameter) was packed with 5 g of BC_{Fe} produced from SB and CH at 300 ºC. The packed column was previously conditioned with 200 mL of HNO$_3$ 0.1 mol/L. As(III) solution (50 mg/L) was supplied at a rate of about 3.5 mL/min. The total volume passed through the system was approximately 1300 mL and aliquots of the solution were collected at 0, 1, 10, 20, 30, 45, 60, 90, 180, 300 and 360 min. As concentration was determined in an ICP-OES.

3. Results and discussion

3.1. Biochars characterisation

The yield of all BC produced from CH and SB was similar (Table A.1, Supplementary Material). On the other hand, the modified biochars (BC_{Fe}) produced at 300 and 400 ºC had smaller yield when they are compared with unmodified biochars. Both biochars BC and BC_{Fe} had similar yield when produced at 500 and 600 ºC.

The smallest yield of biochars with the increase of temperature is related to the volatilisation of organic matter, which leads to an increase in the amount of fixed C and decrease in the amount of H, O (Domingues et al., 2014).

The average of pH$_{zpc}$ found in BC and BC_{Fe} produced from CH and SB at all pyrolysis temperatures (300, 400, 500 and 600 ºC) was 6.05. The results indicate that the surface of these biochars was positively charged (protonated sites) at pH lower than 6.05 and negatively charged at values higher than 6.05. Since As(III) appears mainly as oxyanions in higher pH (> 9.2) and the negative surface of biochars prioritizes its adsorption, the pH 4, 5 and 6 were chosen to perform all experiments (Sharma and Sohn, 2009; Vithanage et al., 2017).

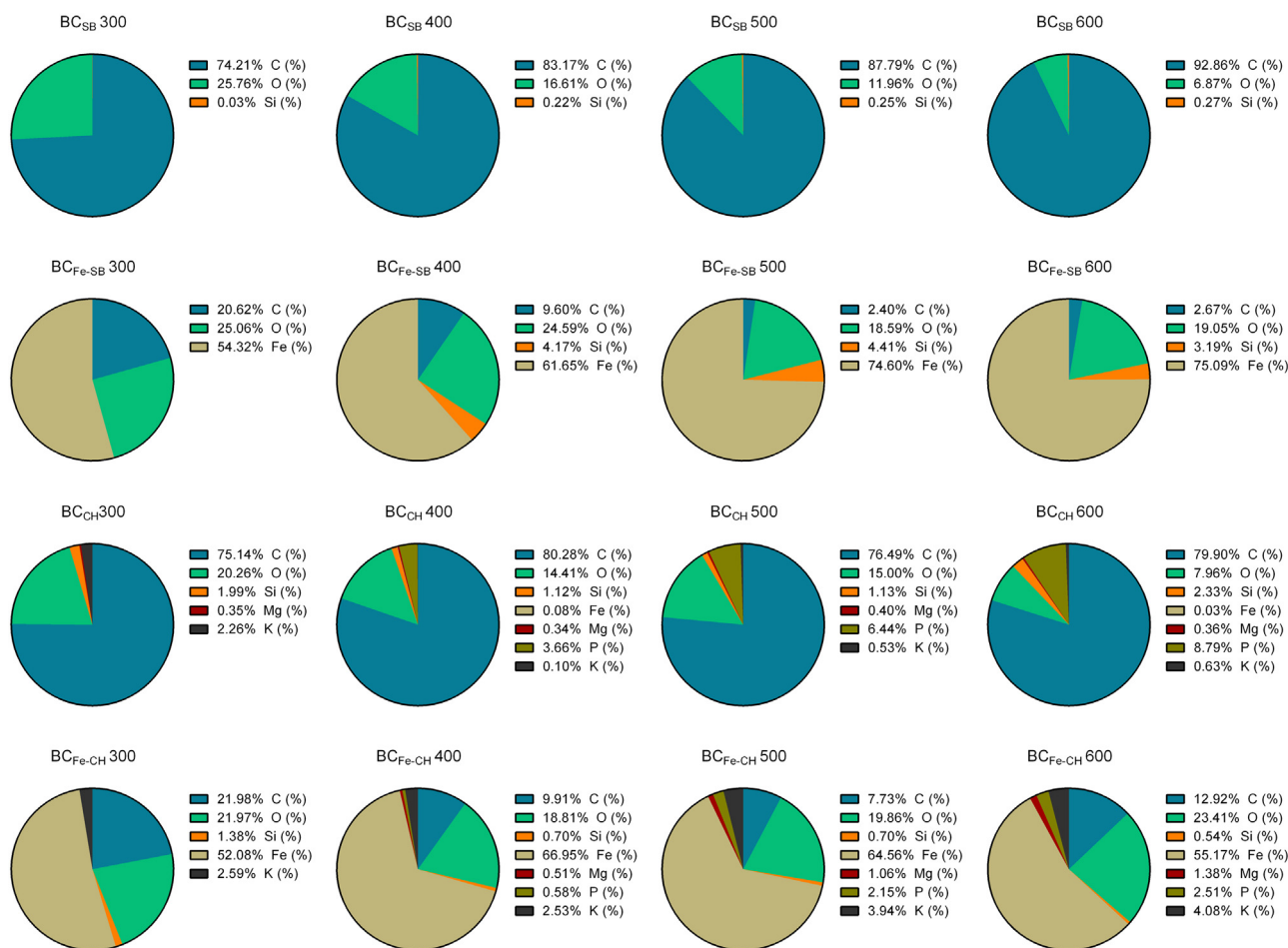The SEM pictures of the BC_{SB} and BC_{CH} produced at 300 ˚C

Fig. 1. Semi-quantitative analysis of elemental composition of the surface of biochars and Fe-coated biochars produced from sugarcane (SB) bagasse and corncob husk (CH) at different temperatures. The suffix indicates the type of biomass used to produce the biochars and the temperature of pyrolysis. All results express the mass percent composition of the elements.

displayed no morphological differences when compared to the samples produced at 400, 500 and 600 °C. However, while the BC_{SB} sample had more definite pores, the BC_{CH} samples had no defined porous structure (see Appendix A, Fig. A.1). Therefore, this indicates that the chosen biomass played an important role in the evolution of the morphological characteristics during pyrolysis treatment.

The SEM images of the Fe-modified biochars (BC_{Fe}) show that the pores observed on the BC_{SB} were impregnated with Fe (Appendix A, Fig. A.2). Consequently, a new type of material was formed and it can be characterised as a colloidal composite (Zhang et al., 2013). The same morphological trend was observed to higher pyrolysis temperatures (500 and 600 °C), as shown in Fig. A.2 in Supplementary Section. Apparently, the micropores were covered with microcrystals of $FeCl_3$.

The EDS analyses of BC and BC_{Fe} from sugarcane bagasse indicate that the elemental composition (semi-quantitative) of the surface of the samples was deeply modified after biomass treatment (Fig. 1). This modification can change the properties of adsorption of the biochars produced, since new functional groups increase the amount of O and Fe on the surface of the Fe-coated biochar after treatment with $FeCl_3$. The BC produced at 400, 500 and 600 °C are similar to the elemental surface composition. In the BC_{Fe} samples, Fe covered most of the surface, since the amount of C decreased in relation to Fe. However, no significant amount of Si in the sample BC_{Fe-SB} was observed at 300 °C.

The same trend of surface modification of BC_{Fe-SB} was observed in BC_{Fe-CH} (Fig. 1). However, some extra elemental modifications were detected in the BC_{CH} and BC_{Fe-CH} since K, Mg and P appeared in external composition depending on the pyrolysis temperature.

The FTIR results reveal that all samples are similar and only small differences related to the type of biomass and treatment with Fe were observed (Fig. A.8, Supplementary Section). The band that appeared around 3100–3400 cm^{-1} is associated to the stretching mode of -OH and it was present especially in the BC_{CH} and BC_{Fe-SB}. The discrete peaks around 1614–1630 cm^{-1} is related to C=O asymmetric stretching of aromatics which was not observed in BC_{Fe-CH}. These last bands decreased or disappeared with the increase of temperature for both biochars (CH and SB) (Baig et al., 2014; Van Vinh et al., 2015). Bands around 1200 and 1000 cm^{-1} are typical of cellulose and hemicellulose due to the C–O and C–N stretching. These bands can also be associated to ashes in elevated temperatures. The bands in the region of 1700 and 1563 cm^{-1} for BC_{Fe-CH} indicate the presence of carbonyl groups of hemicellulose and C–O stretching of carboxyl groups, which reveals interactions with Fe(III) ions (Baig et al., 2014; Van Vinh et al., 2015).

3.2. Adsorption experiments

Although the pH is a key factor in As(III) adsorption, a significant difference among the removal rates was not observed at the pH range used. The Visual MINTEQ results (Fig. A.3 to Fig. A.5, Supplementary Material) showed no As(III) precipitation in any of the experimental conditions. It supports the results of the experiments without adsorbents, where no As precipitation was observed.

The non-modified biochars (BC_{SB} e BC_{CH}) had a small adsorption efficiency (Fig. 2A). On the other hand, the BC_{Fe-SB} produced at 300 °C and all BC_{Fe-CH} adsorbed more than 90% of As(III) at all pH tested
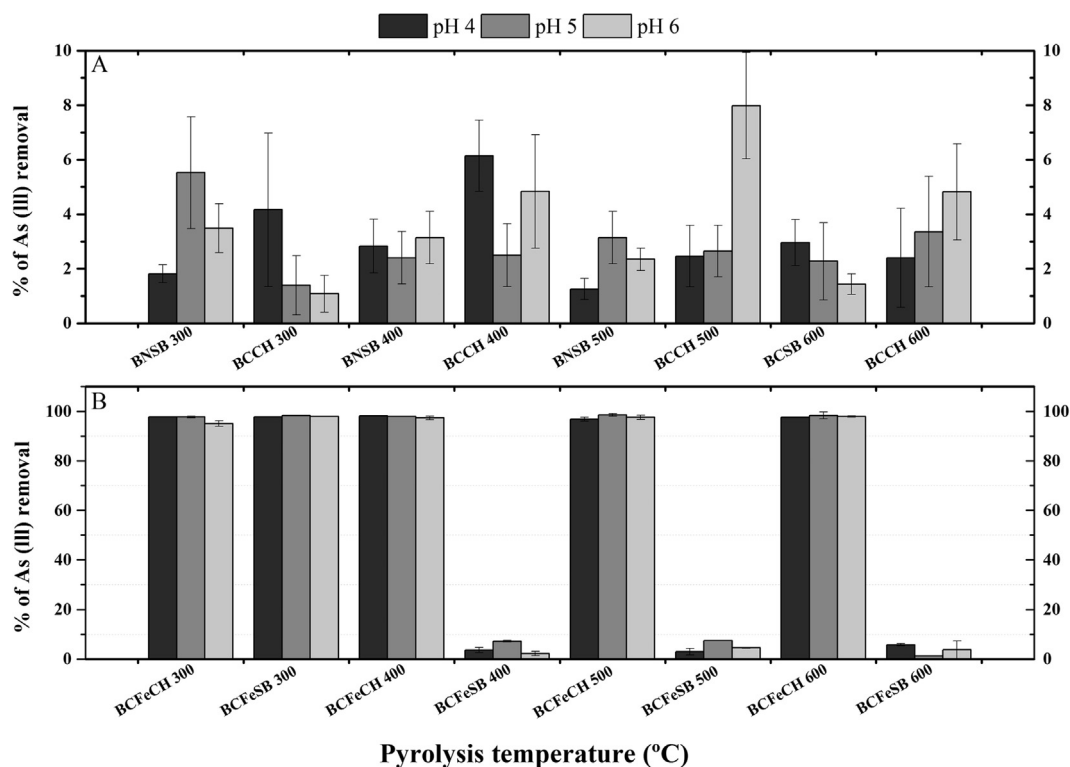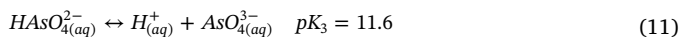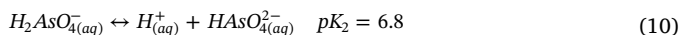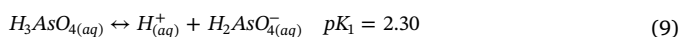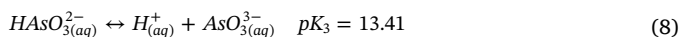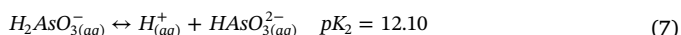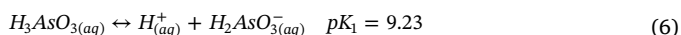
Fig. 2. Removal of As(III) using biochar from corncob husk (CH) and sugarcane bagasse (SB) produced at different temperatures. A: experiments with unmodified biochar (BC); B: experiments with Fe-coated biochar (BC_{Fe}).

(Fig. 2B). This behaviour can be explained by the higher positive charge and modification of functional groups on the biochar surface due to Fe (III) impregnation (Van Vinh et al., 2015; Vithanage et al., 2017).

Since the pH influences the As species distribution, the adsorption mechanisms will be different and more complex depending on the pH of the solution. The different As species and their dissociation constants are shown in Eqs. (6)–(11) (Vithanage et al., 2017; Wei et al., 2016). The higher removal rate by some biochars can be attributed to some neutral and anionic As(III) species. Although the neutral As(III) specie (H_3AsO_3) is the most prevalent and stable in the pH range between 0 and 9, the specie $H_2AsO_4^-$ may also be present. Consequently, both species can bind to biochar (Samsuri et al., 2013; Van Vinh et al., 2015; Vithanage et al., 2017).

$$H_3AsO_{3(aq)} \leftrightarrow H_{(aq)}^+ + H_2AsO_{3(aq)}^- \quad pK_1 = 9.23 \tag{6}$$

$$H_2AsO_{3(aq)}^- \leftrightarrow H_{(aq)}^+ + HAsO_{3(aq)}^{2-} \quad pK_2 = 12.10 \tag{7}$$

$$HAsO_{3(aq)}^{2-} \leftrightarrow H_{(aq)}^+ + AsO_{3(aq)}^{3-} \quad pK_3 = 13.41 \tag{8}$$

$$H_3AsO_{4(aq)} \leftrightarrow H_{(aq)}^+ + H_2AsO_{4(aq)}^- \quad pK_1 = 2.30 \tag{9}$$

$$H_2AsO_{4(aq)}^- \leftrightarrow H_{(aq)}^+ + HAsO_{4(aq)}^{2-} \quad pK_2 = 6.8 \tag{10}$$

$$HAsO_{4(aq)}^{2-} \leftrightarrow H_{(aq)}^+ + AsO_{4(aq)}^{3-} \quad pK_3 = 11.6 \tag{11}$$
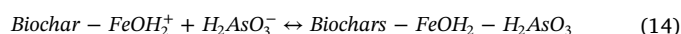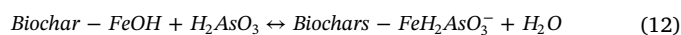
The higher As(III) removal efficiency observed for BC_{Fe} (99.9%, Fig. 2) in relation to BC (6–8%) can be attributed to the formation of new functional groups (higher O content, carboxylic acid-like) and elements such as K, Mg and P as indicated by the EDS analysis (Fig. 1). Consequently, the increasing number of active sites on BC_{Fe} leads to a higher As(III) adsorption on the biochar surface, especially for BC_{Fe-CH}.

Another factor responsible for the higher removal efficiency of all BC_{Fe} is the presence of more positive charges on the surface, which were already positively charged at pH 4, 5 and 6 (see Section 3.1). The introduction of Fe(III) on BC surface enhanced its capacity of

immobilising As(III) through formation of surface complexes with O-containing functional groups or through As interactions with FeOH and $FeOH_2^+$ on the biochar surface. In addition, electrostatic interactions can favour the adsorption of the species H_3AsO_3 on BC_{Fe-SB} and BC_{Fe-CH} (Samsuri et al., 2013; Vithanage et al., 2017).

The FTIR spectra comparing BC_{Fe} and As(III) loaded BC_{Fe} (Fig. A.9, Supplementary Section) were used to better investigate the binding mechanisms of the metalloid in biochar. These spectra showed a change in the size and shape of the bands around $1078 \, cm^{-1}$ (attributed to ester of alcohols and carboxylic acid groups (Asfaram et al., 2016)), which is probably related to ion exchange and/or electrostatic interaction, which supports our former discussions (Niazi et al., 2018a). Shifts in the positions of spectral bands were also observed for the bands around $1580 \, cm^{-1}$ (related to aromatic compounds), which shifts to $1530 \, cm^{-1}$ after As(III) adsorption. Furthermore, the band around $690 \, cm^{-1}$ disappears in the BC_{Fe-SB} loaded by As(III) indicating formation/breaking of chemical bonds. Particularly for the bands below $800 \, cm^{-1}$ these changes are related to Fe-O bond deformations on the BC_{Fe} surface (Kulaksiz et al., 2017).

Experiments of adsorption of the BC_{Fe} at different ionic strengths (Fig. A.7, Supplementary Section) indicate that the amount of adsorbed As(III) decreases when ionic strength increases. It supports the effect of electrostatic attraction in the process of adsorption. Comparing the two types of tested BC_{Fe} with one another, the influence of ionic strength was smaller for BC_{Fe-CH} than for BC_{Fe-SB}. This indicates that groups present in BC_{Fe-CH} have higher affinity to As(III) and form more stable complexes. All possible interactions between BC_{Fe} and As(III) can be described in the Eqs. (12)–(14) (Samsuri et al., 2013; Vithanage et al., 2017):

$$Biochar - FeOH + H_2AsO_3 \leftrightarrow Biochars - FeH_2AsO_3^- + H_2O \tag{12}$$

$$Biochar - FeOH + H_2AsO_3^- \leftrightarrow Biochars - FeHAsO_3^- + H_2O \tag{13}$$

$$Biochar - FeOH_2^+ + H_2AsO_3^- \leftrightarrow Biochars - FeOH_2 - H_2AsO_3 \tag{14}$$

BC_{Fe-CH} was more efficient in the removal of As(III) since a small

mass gets very close to the maximum adsorption when compared with BC_{Fe-SB} (see results in Appendix A, Fig. A.6). In general, as the mass increases, more active sites on biochar surface will be available. Therefore, a higher level of As(III) adsorption would be expected. Nevertheless, in this study a decrease of about 5–12% was detected in As(III) removal when the mass was increased to 0.5 g to both biochars BC_{Fe-SB} and BC_{Fe-CH}. This behaviour can be explained by higher presence of sites of lower energy (Shukla et al., 2002).

3.3. Contact time and adsorption kinetics

Applying kinetic parameters (Table A.2) to the pseudo-second order model fit well to the experimental data (r^2 close to 1.00) derived from both BC_{Fe-SB} and BC_{Fe-CH}. Fitting data of both Fe-coated biochars in this model indicates that the availability of binding sites on the surface of the BC_{Fe} depends on the reaction rate (Vithanage et al., 2017). In addition, the adsorption of As species on both types of BC_{Fe} was fast and the equilibrium time to a complete adsorption was 10 min and the amount of adsorbate at the equilibrium time was 0.72 and 0.96 µg/g to BC_{Fe-SB} and BC_{Fe-CH}, respectively.

The pseudo-first order kinetic model did not fit well in the experimental data and was not considered in this study.

3.4. Adsorption isotherms

Since both BC_{Fe-SB} and BC_{Fe-CH} at pH 4 produced at 300 °C presented excellent adsorption capacities, the isotherms were built in this condition. Fig. 3 presents the Langmuir and Freundlich isotherms for As (III) adsorption on the BC_{Fe} tested as well as the experimental data. The results of the adsorption isotherms were taken from the amount of metalloid adsorbed (µg/g) and the concentration at equilibrium (µg/L). The results show that the Langmuir and Freundlich models presented values close to the ones found in the isotherms. However, Langmuir was the model that best described the As(III) adsorption process in both biochars analysed with higher r^2 (0.97 and 1.00 to BC_{Fe-SB} and BC_{Fe-CH}, respectively) when compared with the Freundlich model. It indicated that adsorption process took place in a monolayer of As(III) onto the surface of both BC_{Fe}, in homogeneous sites specific for biochar. This shows that the adsorption was chemical, with maximum amount of As (III) adsorbed per gram of adsorbent (Q^0) of 20 mg/g and 50 mg/g to BC_{Fe-SB} and BC_{Fe-CH}, respectively.

The materials (SB and CH) used for producing the biochar had good sorption capacity when compared to other materials already studied in the literature. Table 1 compares the best sorption model and maximum sorption capacities for other materials and the type of As used in the tests.

3.5. Desorption experiments

The amounts of desorbed As(III) were 6% and 3% for BC_{Fe-SB} and BC_{Fe-CH}, respectively. The low amount of As(III) desorbed indicates a strong affinity between the metalloid and both types of BC_{Fe}, particularly with BC_{Fe-CH}, which supports the results of the experiments with different ionic strengths (Section 3.2). In addition, the low desorption values indicate that the process is irreversible (do Nascimento et al., 2016).

Although the results suggested that the BC_{Fe} cannot be reused after the first adsorption at the studied conditions, experiments of re-adsorption showed a removal of 75% and 60% of As(III) for BC_{Fe-CH} and BC_{Fe-SB} respectively. It suggests that there were still free binding sites after the first adsorption.

3.6. Commercially activated carbon versus Fe-coated biochar

The results of experiments of As(III) removal by activated carbon compared with BC_{Fe} produced from CH and SB are shown in Fig. 4. The Fe-coated biochars produced from both feedstock had a higher percentage of As(III) removal when compared with commercially activated carbon.

The activated carbon can also be impregnated with Fe as biochar. However, this process would make the process of production even more expensive, which makes the use of Fe-coated biochar a good environmental and economic solution to remove As ions from natural waters and effluents (Vithanage et al., 2017).

3.7. Column leaching experiments

The results of trials with glass columns (Fig. 5) indicates that the commercial use of BC_{Fe-SB} and BC_{Fe-CH} for As(III) removal is practicable, since both adsorbents had good removal rates (99% and 96% respectively). Moreover, it was demonstrated that the adsorption process is fast (10 min for BC_{Fe-SB} and 30 min for BC_{Fe-CH}) and the contact time
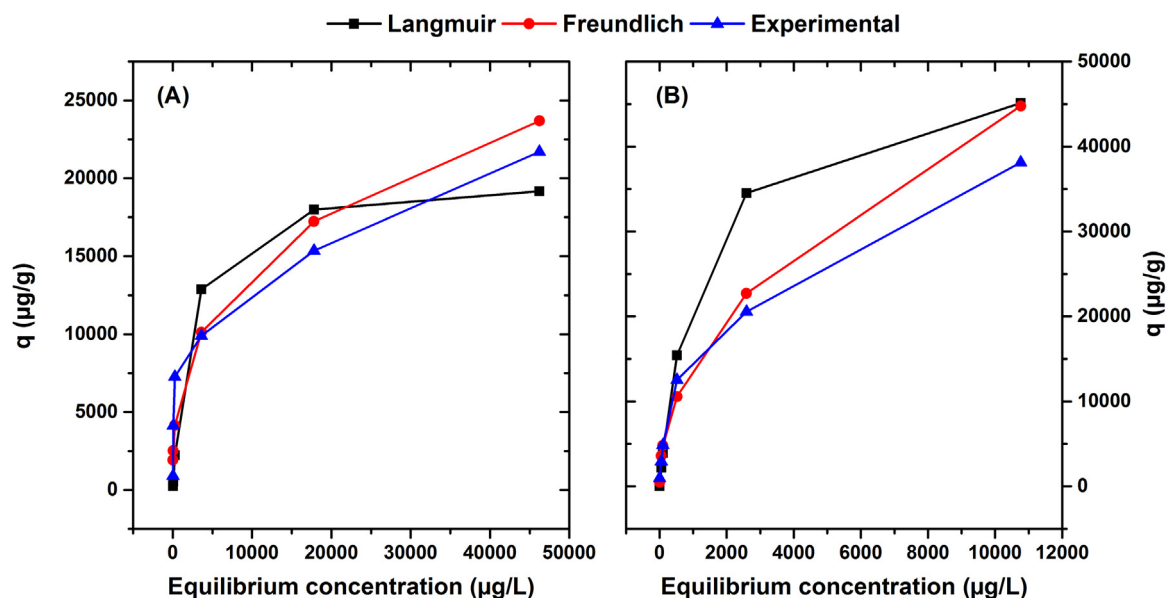

Fig. 3. Langmuir, Freundlich and experimental plot for the adsorption of As(III) by Fe-coated biochars (BC_{Fe}) produced from (A) sugarcane bagasse (SB) and (B) corncob husk (CH). Both SB and CH biochars were produced at 300 °C.

Table 1
Comparison among biochars produced from different materials in the removal of As.

| Biomass type	As type	Best sorption model	Best pH	Maximum sorption capacity of biochar (mg/g)	Reference
Sugarcane bagasse (SB) and corncob husk (CH) coated with Fe	As(III)	Langmuir	4	20 for SB coated with Fe and 50 for CH coated with Fe	This study
Japanese oak wood	As(III) / As (V)	Langmuir	7.3 for As(III) / 6.21 for As(V)	3.21 for As(III) / 3.39 for As(V) (92–100% of total As was removed for natural contaminated ground water)	Niazi et al. (2018b)
Oil palm empty fruit bunch (EFB) and rice husk (RH) (non-modified and coated with Fe)	As(III) / As (V)	Langmuir	8 and 9 for As(V) and all sorbents tested	18.9 and 19.3 for EFB and RH for As(III) / 5.5 and 7.1 for EFB and RHB for As(V). Fe coated biochars: 31.4 and 30.7 for EFB and RH for As(III). 15.2 and 16.0 for EFB and RHB for As(V)	Samsuri et al. (2013)
Oak wood, pine wood, oak bark and pine bark	As(III)	Freundlich and Langmuir	3–4	Oak wood (5.85), pine wood (1.20), oak bark (7.40) and pine bark (12.15)	Mohan et al. (2007)
Pinewood (PW) and pinewood treated with hematite (HPW)	As(V)	Langmuir	Not tested. Experiments performed at pH 7	0.265 for PW and 0.429 for HPW	Wang et al. (2015)
Rice husk (RH), the organic fraction of municipal solid wastes (SW) and sewage sludge (SS)	As(V)	Freundlich	Not tested. Experiments performed at pH 9.5	25% of As removal for RH, 53% for SS and 55% for SW	Agrafioti et al. (2014)
Cotton wood coated with Fe (γ-Fe$_2$O$_3$)	As(V)	Langmuir	–	3.147 for biochar/γ-Fe$_2$O$_3$ composite	Zhang et al. (2013)
Pine cones (PC) and PC loaded with Zn	As(III)	Langmuir	2–4	0.0057 for PC and 0.007 for the Zn loaded biochar	Van Vinh et al. (2015)
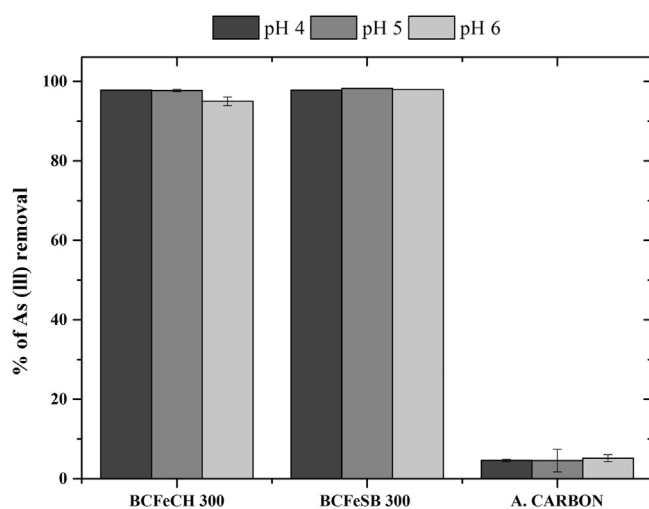
Fig. 4. Comparing As(III) adsorption on commercially activated carbon and Fe-coated (BC$_{Fe}$) biochars produced from sugarcane bagasse (SB) and corncob husk (CH). All BC$_{Fe}$ produced at 300 °C and the experiments performed at pH 4.
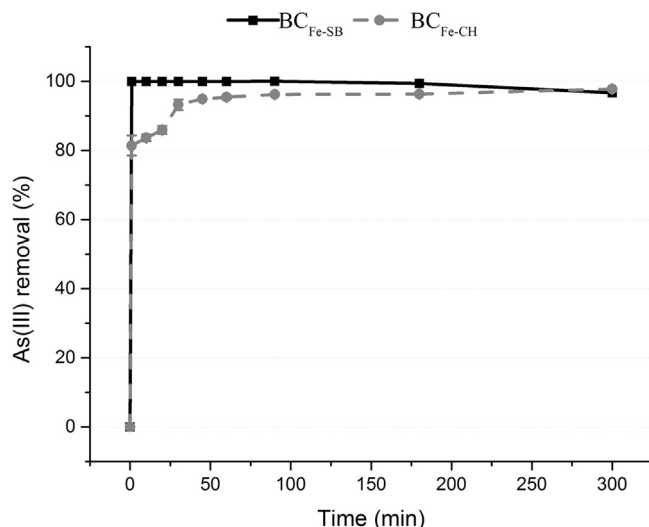

Fig. 5. Column leaching experiments results. The columns were packed either with BC$_{Fe-SB}$ or BC$_{Fe-CH}$.

was enough to remove nearly all As(III) from high concentration solutions (50 mg/L). The fast kinetics is attractive for both *in situ* remediation and use in filters applications, since time and efficiency are required in new technologies.

4. Conclusions

The modification of BC produced from SB and CH with Fe(III) improved significantly As(III) adsorption (> 99%). However, the BC$_{Fe-CH}$ was highly efficient for all pyrolysis temperatures, while BC$_{Fe-SB}$ had good removal results only when produced at 300 °C. The process of As (III) adsorption had fast kinetics (10–30 min) and it was better adjusted to pseudo-second order and Langmuir models. The maximum adsorption capacity was superior to other studies in literature (20 mg/g for BC$_{Fe-SB}$ and 50 mg/g for BC$_{Fe-CH}$). Batch and column desorption experiments showed that the adsorption process is almost irreversible. However, tests of re-adsorption indicated that there were still binding sites available, but the removal rates were 20–30% smaller than in the first adsorption-desorption phase.

The fast removal process makes the BC$_{Fe-CH}$ and BC$_{Fe-SB}$ attractive for *in situ* and commercial (filters) use, since time and efficiency are

required in new technologies. The use of BC as an adsorbent to remove As(III) is cheap, which makes its usage particularly advantageous when compared to other traditional techniques (activated carbon for instance). In addition, there are other benefits related to reuse of leftovers of biomass produced in large amounts in countries like Brazil and China. The disposal of these residues in the fields may pose risks to crops, such as fire or delay in plant development.

Appendix A. Supplementary material

Supplementary data associated with this article can be found in the online version at doi:10.1016/j.ecoenv.2018.07.042.

References

Agrafioti, E., et al., 2014. Arsenic and chromium removal from water using biochars derived from rice husk, organic solid wastes and sewage sludge. J. Environ. Manag. 133, 309–314.

Ahn, J.S., et al., 2003. Arsenic removal using steel manufacturing byproducts as permeable reactive materials in mine tailing containment systems. Water Res. 37, 2478–2488.

Asfaram, A., et al., 2017a. Ultrasound-assisted binary adsorption of dyes onto Mn@ CuS/ZnS-NC-AC as a novel adsorbent: application of chemometrics for optimization and modeling. J. Ind. Eng. Chem. 54, 377–388.

Asfaram, A., et al., 2018. Preparation and characterization of Mn0.4Zn0.6Fe2O4 nanoparticles supported on dead cells of yarrowia lipolytica as a novel and efficient adsorbent/biosorbent composite for the removal of azo food dyes: central composite design optimization study. ACS Sustain. Chem. Eng. 6, 4549–4563.

Asfaram, A., et al., 2016. Biosorption of Zn2+, Ni2+ and Co2+ from water samples onto Yarrowia lipolytica ISF7 using a response surface methodology, and analyzed by inductively coupled plasma optical emission spectrometry (ICP-OES). RSC Adv. 6, 23599–23610.

Asfaram, A., et al., 2017b. Application of experimental design and derivative spectrophotometry methods in optimization and analysis of biosorption of binary mixtures of basic dyes from aqueous solutions. Ecotoxicol. Environ. Saf. 139, 219–227.

Asfaram, A., et al., 2015. Response surface methodology approach for optimization of simultaneous dye and metal ion ultrasound-assisted adsorption onto Mn doped Fe3O4-NPs loaded on AC: kinetic and isothermal studies. Dalton Trans. 44, 14707–14723.

Azizur Rahman, M., Hasegawa, H., 2012. Arsenic in freshwater systems: influence of eutrophication on occurrence, distribution, speciation, and bioaccumulation. Appl. Geochem. 27, 304–314.

Baig, S.A., et al., 2014. Effect of synthesis methods on magnetic Kans grass biochar for enhanced As(III, V) adsorption from aqueous solutions. Biomass Bioenergy 71, 299–310.

Ballinas, M. d.L., et al., 2004. Arsenic(V) removal with polymer inclusion membranes from sulfuric acid media using DBBP as carrier. Environ. Sci. Technol. 38, 886–891.

Bazrafshan, A.A., et al., 2017. Synthesis of ZnO-nanorod-based materials for antibacterial, antifungal activities, DNA cleavage and efficient ultrasound-assisted dyes adsorption. Ecotoxicol. Environ. Saf. 142, 330–337.

Budinova, T., et al., 2006. Removal of arsenic(III) from aqueous solution by activated carbons prepared from solvent extracted olive pulp and olive stones. Ind. Eng. Chem. Res. 45, 1896–1901.

Bueno, C.C., et al., 2017. Investigation on prospective energy power from corncob husk biomass and its biochars by kinetic parameters and isoconversional models. J. Braz. Chem. Soc.

Chandra, V., et al., 2010. Water-dispersible magnetite-reduced graphene oxide composites for arsenic removal. ACS Nano. 4, 3979–3986.

Choong, T.S.Y., et al., 2007. Arsenic toxicity, health hazards and removal techniques from water: an overview. Desalination 217, 139–166.

Corapcioglu, M.O., Huang, C.P., 1987. The surface acidity and characterization of some

commercial activated carbons. Carbon 25, 569–578.

Cumbal, L., et al., 2003. Polymer supported inorganic nanoparticles: characterization and environmental applications. React. Funct. Polym. 54, 167–180.

Dambies, L., 2005. Existing and prospective sorption technologies for the removal of arsenic in water. Sep. Sci. Technol. 39, 603–627.

Diamadopoulos, E., et al., 1993. As(V) removal from aqueous solutions by fly ash. Water Res. 27, 1773–1777.

do Nascimento, F.H., et al., 2016. Evaluation of thiol-modified vermiculite for removal of Hg(II) from aqueous solutions. Appl. Clay Sci. 124–125, 227–235.

Dominguez, M.T., et al., 2014. Polymeric alginate microspheres containing biochar to immobilize phosphate ions. Chem. Eng. Trans. 37, 109–114.

Dong, C.-D., et al., 2018. Wood-biochar-supported magnetite nanoparticles for remediation of PAH-contaminated estuary sediment. Catalysts 8, 73.

Genç, H., et al., 2003. Adsorption of arsenate from water using neutralized red mud. J. Colloid Interface Sci. 264, 327–334.

Ghimire, K.N., et al., 2002. Effectiveness of phosphorylated orange residue for toxic oxoanion removal. Des. Monomers Polym. 5, 401–414.

Gihring, T.M., et al., 2001. Rapid arsenite oxidation by thermus aquaticus and thermus thermophilus: field and laboratory investigations. Environ. Sci. Technol. 35, 3857–3862.

Guo, X., Chen, F., 2005. Removal of arsenic by bead cellulose loaded with iron oxyhydroxide from groundwater. Environ. Sci. Technol. 39, 6808–6818.

Gupta, V.K., et al., 2005. Adsorption of As(III) from aqueous solutions by iron oxide-coated sand. J. Colloid Interface Sci. 288, 55–60.

Haron, M.J., Yunus, M.Z.W., Sukari, M.A., Wum, L.T., Tokugana, S., 1997. Removal of arsenic(V) by cerium(III) complexed chelating ion exchanger. The Malaysian. J. Anal. Sci. 3, 193–204.

Hering, J.G.C., Pen-Yuan, Wilkie, Jennifer A., Elimelech, Menachem, Liang, Sun, 1996. Arsenic removal by ferric chloride. J. Am. Water Works Assoc. 88, 155–167.

Ho, Y.S., McKay, G., 1999. Pseudo-second order model for sorption processes. Process Biochem. 34, 451–465.

Huang, W., et al., 1998. Hysteresis in the sorption and desorption of hydrophobic organic contaminants by soils and sediments: 1. A comparative analysis of experimental protocols. J. Contam. Hydrol. 31, 129–148.

Jain, C.K., Ali, I., 2000. Arsenic: occurrence, toxicity and speciation techniques. Water Res. 34, 4304–4312.

Kim, D.H., et al., 2006a. Removal and transport mechanisms of arsenics in UF and NF membrane processes. J. Water Health 4, 215–223.

Kim, J., et al., 2006b. Arsenic removal from water using lignocellulose adsorption medium (LAM). J. Environ. Sci. Health A Tox Hazard Subst. Environ. Eng. 41, 1529–1542.

Kordmostafapour, F., et al., 2006. Arsenic removal by dissolved air flotation. J. Appl. Sci. 6, 1153–1158.

Kulaksiz, E., et al., 2017. Adsorption of Malachite Green on Fe-modified biochar: influencing factors and process optimization. Desalin. Water Treat. 74, 383–394.

Lata, S., Samadder, S.R., 2016. Removal of arsenic from water using nano adsorbents and challenges: a review. J. Environ. Manag. 166, 387–406.

Leão, G.A., et al., 2017. Phytoremediation of arsenic-contaminated water: the role of antioxidant metabolism of Azolla caroliniana Willd. (Salviniales). Acta Bot. Bras. 31, 161–168.

Manochio, C., et al., 2017. Ethanol from biomass: a comparative overview. Renew. Sustain. Energy Rev. 80, 743–755.

Mayo, J.T., et al., 2007. The effect of nanocrystalline magnetite size on arsenic removal. Sci. Technol. Adv. Mater. 8, 71–75.

Mohan, D., Chander, S., 2006. Removal and recovery of metal ions from acid mine drainage using lignite—a low cost sorbent. J. Hazard. Mater. 137, 1545–1553.

Mohan, D., et al., 2014. Cadmium and lead remediation using magnetic oak wood and oak bark fast pyrolysis bio-chars. Chem. Eng. J. 236, 513–528.

Mohan, D., et al., 2007. Sorption of arsenic, cadmium, and lead by chars produced from fast pyrolysis of wood and bark during bio-oil production. J. Colloid Interface Sci. 310, 57–73.

Moraes, M.S.A., et al., 2012. Analysis of products from pyrolysis of Brazilian sugar cane straw. Fuel Process. Technol. 101, 35–43.

Morin, G., Calas, G., 2006. Arsenic in soils, mine tailings, and former industrial sites. Elements 2, 97–101.

Muñoz, J.A., et al., 2002. Arsenic adsorption by Fe(III)-loaded open-celled cellulose sponge. Thermodynamic and selectivity aspects. Environ. Sci. Technol. 36, 3405–3411.

Natarajan, S., et al., 2011. Phytoremediation of arsenic-contaminated groundwater using arsenic hyperaccumulator Pteris vittata L.: effects of frond harvesting regimes and arsenic levels in refill water. J. Hazard Mater. 185, 983–989.

Niazi, N.K., et al., 2018a. Arsenic removal by perilla leaf biochar in aqueous solutions and groundwater: an integrated spectroscopic and microscopic examination. Environ. Pollut. 232, 31–41.

Niazi, N.K., et al., 2018b. Arsenic removal by Japanese oak wood biochar in aqueous solutions and well water: investigating arsenic fate using integrated spectroscopic and microscopic techniques. Sci. Total Environ. 621, 1642–1651.

Nidheesh, P.V., Singh, T.S.A., 2017. Arsenic removal by electrocoagulation process: recent trends and removal mechanism. Chemosphere 181, 418–432.

Pacheco, A.C.C., Torem, M.L., 2002. Influence of ionic strength on the removal of As(V) by adsorption colloid flotation. Sep. Sci. Technol. 37, 3599–3610.

Pokhrel, D., Viraraghavan, T., 2006. Arsenic removal from an aqueous solution by a modified fungal biomass. Water Res. 40, 549–552.

Pollard, S.J.T., et al., 1992. Low-cost adsorbents for waste and wastewater treatment: a review. Sci. Total Environ. 116, 31–52.

Qu, X., et al., 2013. Applications of nanotechnology in water and wastewater treatment.

Water Res. 47, 3931–3946.

Ramakrishna, D.M., Viraraghavan, T., Jin, Y.-C., 2006. Coated sand for arsenic removal: investigation of coating parameters using factorial design approach. Periodical of Hazardous, Toxic, and Radioactive. Waste Manag. 10, 198–206.

Ratna Kumar, P., et al., 2004. Removal of arsenic from water by electrocoagulation. Chemosphere 55, 1245–1252.

Samsuri, A.W., et al., 2013. Adsorption of As(III) and As(V) by Fe coated biochars and biochars produced from empty fruit bunch and rice husk. J. Environ. Chem. Eng. 1, 981–988.

Sharma, V.K., Sohn, M., 2009. Aquatic arsenic: toxicity, speciation, transformations, and remediation. Environ. Int. 35, 743–759.

Shukla, A., et al., 2002. The role of sawdust in the removal of unwanted materials from water. J. Hazard. Mater. 95, 137–152.

Smedley, P.L., Kinniburgh, D.G., 2002. A review of the source, behaviour and distribution of arsenic in natural waters. Appl. Geochem. 17, 517–568.

Soner Altundoğan, H., et al., 2000. Arsenic removal from aqueous solutions by adsorption on red mud. Waste Manag. 20, 761–767.

Thakur, L.S., Mondal, P., 2017. Simultaneous arsenic and fluoride removal from synthetic and real groundwater by electrocoagulation process: parametric and cost evaluation. J. Environ. Manag. 190, 102–112.

Ungureanu, G., et al., 2015. Arsenic and antimony in water and wastewater: overview of removal techniques with special reference to latest advances in adsorption. J. Environ. Manag. 151, 326–342.

Van Vinh, N., et al., 2015. Arsenic(III) removal from aqueous solution by raw and zinc-loaded pine cone biochar: equilibrium, kinetics, and thermodynamics studies. Int. J. Environ. Sci. Technol. 12, 1283–1294.

Vithanage, M., et al., 2017. Interaction of arsenic with biochar in soil and water: a critical review. Carbon 113, 219–230.

Wang, S., et al., 2015. Removal of arsenic by magnetic biochar prepared from pinewood and natural hematite. Bioresour. Technol. 175, 391–395.

Wang, S., Mulligan, C.N., 2006. Natural attenuation processes for remediation of arsenic contaminated soils and groundwater. J. Hazard. Mater. 138, 459–470.

Wang, S., Peng, Y., 2010. Natural zeolites as effective adsorbents in water and wastewater treatment. Chem. Eng. J. 156, 11–24.

Wei, Z., et al., 2016. The effect of pH on the adsorption of arsenic(III) and arsenic(V) at the TiO2 anatase [101] surface. J. Colloid Interface Sci. 462, 252–259.

Zhang, F.-S., Itoh, H., 2005. Iron oxide-loaded slag for arsenic removal from aqueous system. Chemosphere 60, 319–325.

Zhang, H., et al., 2010. Effect of Pinus radiata derived biochars on soil sorption and desorption of phenanthrene. Environ. Pollut. 158, 2821–2825.

Zhang, M., et al., 2013. Preparation and characterization of a novel magnetic biochar for arsenic removal. Bioresour. Technol. 130, 457–462.